Journal of Biomedical Optics

BiomedicalOptics.SPIEDigitalLibrary.org

Spatial distributions of hemoglobin signals from superficial layers in the forehead during a verbal-fluency task

Satoru Kohno
Yoko Hoshi

SPIE.

Satoru Kohno, Yoko Hoshi, "Spatial distributions of hemoglobin signals from superficial layers in the forehead during a verbal-fluency task," *J. Biomed. Opt.* **21**(6), 066009 (2016), doi: 10.1117/1.JBO.21.6.066009.

Spatial distributions of hemoglobin signals from superficial layers in the forehead during a verbal-fluency task

Satoru Kohno[a,b,*] and Yoko Hoshi[b,c]
[a]Tokushima University, Graduate School of Biomedical Sciences, Department of Radiation Science and Technology, Division of Radiological Sciences, 3-18-15 Kuramoto-cho, Tokushima 770-8503, Japan
[b]Tokyo Metropolitan Institute of Medical Science, Integrated Neuroscience Research Project, 2-1-6 Kamikitazawa, Setagaya-ku, Tokyo 156-8506, Japan
[c]Hamamatsu University School of Medicine, Preeminent Medical Photonics Education and Research Center, Institute for Medical Photonics Research, Department of Biomedical Optics, 1-20-1 Handayama, Higashi-ku, Hamamatsu 431-3192, Japan

Abstract. Functional near-infrared spectroscopy (fNIRS) signals originate in hemoglobin changes in both the superficial layer of the head and the brain. Under the assumption that the changes in the blood flow in the scalp are spatially homogeneous in the region of interest, a variety of methods for reducing the superficial signals has been proposed. To clarify the spatial distributions of the superficial signals, the superficial signals from the forehead during a verbal-fluency task were investigated by using ten source–detector pairs separated by 5 mm, whereas fNIRS signals were also detected from two source–detector pairs separated by 30 mm. The fNIRS signals strongly correlated with the superficial signals at some channels on the forehead. Hierarchical cluster analysis was performed on the temporal cross-correlation coefficients for two channels of both the NIRS signals, and the analysis results demonstrate spatially heterogeneous distributions and network structures of the superficial signals from within the forehead. The results also show that the assumption stated above is invalid for homogeneous superficial signals from any region of interest of 15-mm diameter or larger on the forehead. They also suggest that the spatially heterogeneous distributions may be attributable to vascular networks, including supraorbital, supratrochlear, and superficial temporal vessels. [DOI: 10.1117/1.JBO.21.6.066009]

Keywords: functional near-infrared spectroscopy; verbal-fluency task; superficial signals; blood flow; supraorbital; cluster analysis.

Paper 160047R received Jan. 27, 2016; accepted for publication May 23, 2016; published online Jun. 14, 2016.

1 Introduction

Near-infrared spectroscopy (NIRS) can estimate relative changes in tissue oxygenated hemoglobin (oxy-Hb) and deoxygenated hemoglobin (deoxy-Hb) noninvasively by irradiating near-infrared light on the surface of the body and detecting the reflecting light emerging a few centimeters from the incident position.[1–3] This technique was originally designed for clinical monitoring of tissue oxygenation, and it has also been developed into a useful tool in neuroimaging studies, with so-called functional near-infrared spectroscopy (fNIRS), which estimates the changes in cerebral Hb associated with hemodynamic responses to neuronal activation.[4–7] Since fNIRS has several advantages over other imaging techniques, such as portability and fewer physical restrictions, it has now found a wide range of applications in the field of brain science (e.g., cognitive neuroscience,[8–12] motor rehabilitation,[13–18] and neuropsychiatric disorders[19–23]). However, the fNIRS signal is extremely vulnerable to contamination by hemodynamic changes in the superficial layers of the head (i.e., the skin, skull, and cerebrospinal fluid), because the sensitivity of the fNIRS signal to hemoglobin changes in the superficial layers is around 20 times higher than to that in deeper layers (i.e., the brain).[24]

It has been already shown that the fNIRS signal is contaminated by task-related hemoglobin changes in the skin blood flow during a locomotor task on a treadmill.[25] It has also been reported that such fNIRS signal contamination occurred in all measurement areas on the forehead during a verbal-fluency task (VFT).[26] This report made a striking impact on the fNIRS community, since fNIRS measurements on the forehead during a VFT had been approved as one of the "advanced medical technologies" for aiding differential diagnosis of depressive symptoms by the Ministry of Health, Labor, and Welfare of Japan in 2009.[27]

To reduce the fNIRS signal contamination, numerous methods have been proposed. They can be categorized as methods that (1) use data postprocessing based on physiological differences between cerebral and skin hemoglobin signals,[25,28] (2) use some additional short-distance channels other than the fNIRS channels,[29–33] and (3) analyze temporal profiles of photons detected by time-resolved spectroscopy.[2,34,35] As for these methods, a variety of assumptions has been made. One of the most common assumptions made in regard to methods (1) and (2) is that a task-related superficial NIRS signal is spatially homogeneous across the scalp and forehead. However, this assumption has not yet been validated.

Localization, time course, and physiological origin of task-evoked superficial fNIRS signals during a continuous performance task (CRT) have recently been examined.[36] It was observed that the sources of the task-evoked systemic fNIRS

*Address all correspondence to: Satoru Kohno, E-mail: kohno@medsci.tokushima-u.ac.jp

1083-3668/2016/$25.00

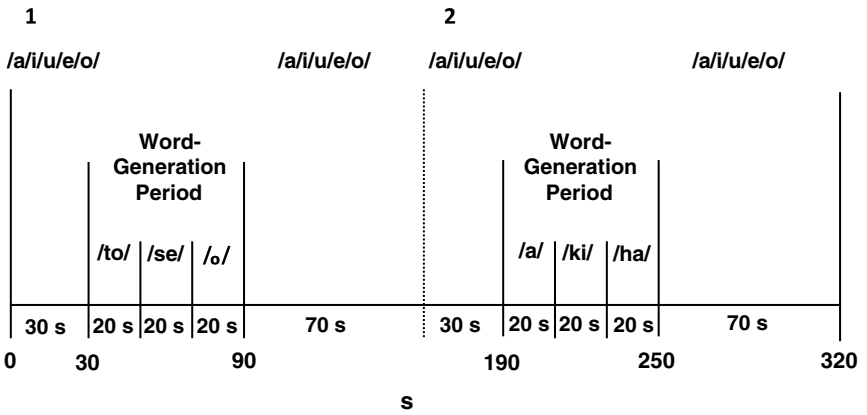

Fig. 1 A letter-cued VFT consisting of two blocks. Each block consisted of a 60-s-long word-generation period that was preceded for 30 s and followed for 70 s by control periods. During the word-generation periods, the participant had to generate as many words as possible that started with a character that was displayed every 20 s. During the control periods, the participant was instructed to repeat five vowels: /a/, /i/, /u/, /e/, and /o/.

signals are colocalized with draining of veins in the scalp, and the physiological origin of a systemic artifact is a task-evoked sympathetic arterial vasoconstriction followed by a decrease in venous volume.[36] However, unlike the VFT and other cognitive tasks, the CRT was accompanied by decreases in the intensity of fNIRS signals. The findings of that study, therefore, might have been specific to the CRT. It has also been shown that the correlation between baseline NIRS signals measured at two different locations on the left motor area decreases as the relative distance between the two measurements increases. This finding indicated that a superficial NIRS signal is spatially inhomogeneous.[37] However, the inhomogeneous distribution has not been directly confirmed by assessing task-related superficial signals.

The aim of this study is to clarify the distribution pattern of task-related superficial signals. First, the hemoglobin signals in the superficial layer of the forehead during a VFT were collected from 10 source–detector pairs at a short separation of 5 mm. Second, the temporal cross correlations of the oxy-Hb between any two channels were calculated, and the calculated correlations were subjected to cluster analysis.

2 Materials and Methods

2.1 *Subjects*

Sixteen healthy volunteers [12 males, 4 females, mean age ± standard deviation (SD), 27.1 ± 11.0 years] participated in this study. All had no history of neurological or psychiatric disorders, and written informed consent was obtained from all of them. This study was approved by the ethics committee of Tokyo Metropolitan Institute of Medical Science.

2.2 *Letter-Cued Verbal-Fluency Task*

The letter-cued VFT, which consisted of two blocks (Fig. 1), was used to induce hemodynamic changes.[26] Each block consisted of a 60-s-long word-generation period that was preceded for 30 s and followed for 70 s by control periods (Fig. 1). During the control periods, participants were instructed to repeat the five Japanese vowels: /a/, /i/, /u/, /e/, and /o/ (the first five letters in the Japanese alphabet), at a rate of approximately one syllable per second. During the word-generation period, three characters of the Japanese phonetic syllables called *hiragana* were displayed on the computer screen one-by-one with an interval of 20 s, and the subjects had to generate and announce as many words as possible in the 20-s period that started with each character. Three phonetic characters, pronounced as /to/, /se/, and /o/, were displayed in that order in one block, and three others, /a/, /ki/, and /ha/, were displayed in the other. In addition, to avoid any moving and gaze shifting artifacts, the subjects were instructed to look at the crosshair in the middle of the computer screen during the control periods and not to shift their gaze during the task period.

2.3 *Data Acquisition*

The subjects sat on a comfortable chair in the examination room. A video-monitoring system and an audio system were used to monitor the subject's movements and count the number of correctly generated words during the 60-s activation period, which was defined as the task performance.[38] A multichannel continuous-wave NIRS imaging system (FOIRE 3000, Shimadzu Corp., Kyoto, Japan), which employs three laser diodes at differing wavelengths (780, 805, and 830 nm) as light sources, was used. The arrangements and positions of the light sources, detectors, and the corresponding channels are shown in Fig. 2. It has been reported that more than 99.6% of photons detected at a source–detector distance of 5 mm do not reach the gray matter of the brain in any adults.[26] Thus, to measure hemoglobin signals from the superficial layer, 10 source–detector pairs (T1-R1, T2-R2, T3-R3, T4-R4, T5-R5, T6-R6, T7-R7, T8-R8, T9-R9, and T10-R10) with a short separation of 5 mm (NEAR channels) were placed on the horizontal line of the forehead 35 mm above the nasion. In addition, to measure fNIRS signals, which are defined as those arising from both the extracerebral and cerebral tissue (BA10), two detectors (R11 and R12) were placed at a source–detector separation of 40 mm from T1 and T6 (FAR channels), respectively. To achieve this optode arrangement, a special small optode (length: 10 mm, wide: 5 mm, and thickness: 3 mm) is used in our experiments. The optodes were firmly fixed on the forehead using a pressure-sensitive adhesive sheet.

Each detection optical fiber in the NIRS imaging system was connected to a photomultiplier tube, the sensitivity of which was tuned at the three above-mentioned wavelengths. During signal acquisition, each of the three laser diodes sequentially delivered a 5-ms pulse of light to a source fiber, followed by 10-ms intervals of dark signal acquisition. In this study, the laser lights from

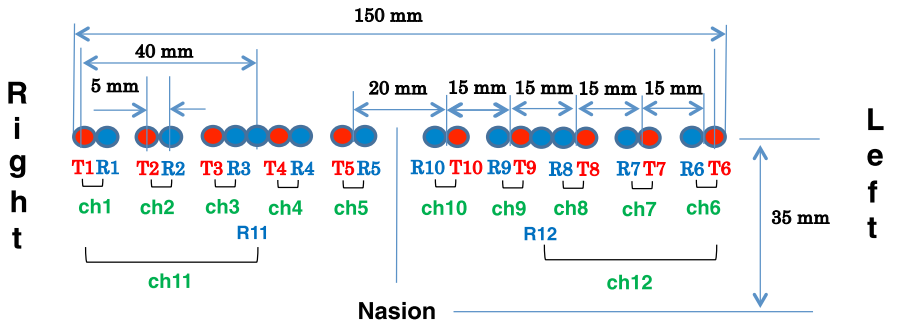

Fig. 2 Illustration of optodes for measuring superficial-layer signals. Ten source–detector pairs (T1-R1, T2-R2, T3-R3, T4-R4, T5-R5, T6-R6, T7-R7, T8-R8, T9-R9, and T10-R10) with a short separation of 5 mm were placed on the horizontal line of the forehead 35 mm above the nasion. Two additional detectors (R11 and R12) were placed with a source–detector separation of 40 mm for T1 and T6, respectively.

the 10 source optical fibers (T1 to T10) were emitted sequentially. As a result, signals at all the 12 channels were obtained every 160 ms.

3 Data Analysis

3.1 *Preprocessing*

Oxy-Hb and deoxy-Hb signals were calculated by solving a simultaneous equation from the modified Beer–Lambert's law[39] with a set of molecular absorption coefficients[40] and the absorbance changes at three wavelength (780, 805, and 830 nm) as measured by the NIRS system.[25] The modified Beer–Lambert's law is expressed as $A = -\log I/I_0 = \varepsilon CBL + G$, where A is the attenuation measured in optical density, I and I_0 are the intensities of the detected and incident light, ε is the molar absorption coefficient, C is the concentration of chromophore (e.g., Hb), B is a pathlength factor dependent upon the absorption and scattering coefficients and the scattering phase function, L is the interoptode distance between the source and detector, and G is an unknown geometry-dependent factor.[39] The oxy-Hb and the deoxy-Hb signals were preprocessed using 85-points cubic Savitzky–Golay smoothing.[41] Although some recent studies have suggested that deoxy-Hb signals are more sensitive to activity-related changes in regional cerebral blood flow, oxy-Hb signals have exclusively been investigated in fNIRS studies, because deoxy-Hb signals have been thought to be unreliable due to their low-signal intensities and nonnegligible cross talk errors.[42] It has also been reported that oxy-Hb signals are significantly contaminated by extracranial signals, whereas deoxy-Hb signals are not.[36] Thus, the oxy-Hb signals were analyzed to examine the spatial distribution pattern of skin blood flow changes.

3.2 *Temporal Cross Correlations Between Near-Infrared Spectroscopy Signals*

The relationships between the oxy-Hb signals obtained from the fNIRS (two channels) and those from the superficial layer (10 channels) on the forehead during the letter-cued VFT were examined first. For this purpose, the 20 (2 channels × 10 channels) temporal cross-correlation matrix elements between these signals were calculated. In addition, to investigate spatial distributions of the oxy-Hb signals from the superficial layer in the forehead during the task, the 45 (the number of combinations of 2 channels from the 10 channels) temporal cross-correlation matrix elements for the 10 channels of the superficial layer were calculated.

3.3 *Coefficients of Spatial Distributions*

To evaluate spatial distributions of the oxy-Hb signals in the superficial layers, a new statistical value, namely, the coefficient of spatial uniformity (CSU) is defined as

$$\mathrm{CSU} = \langle r \rangle / \sigma, \tag{1}$$

where $\langle r \rangle$ and σ are, respectively, the arithmetic mean and SD of the 45 temporal cross-correlation coefficients between the oxy-Hb signals in the superficial layer.

3.4 *Hierarchical Variable Cluster Analysis*

To investigate the characteristics of the temporal cross correlations of the measured NIRS signals on the 12 channels, the temporal cross correlations were hierarchically clustered by using the PROC VARCLUS procedure of the software package SAS (SAS/STAT, Cary, NC, 13.2 User's guide The VARCLUS Procedure[43]).

The VARCLUS procedure is a method of directly clustering correlation matrices. The VARCLUS algorithm begins with all variables in a single cluster, and repeats the following steps.

1. Principal-component analysis determines whether the selected cluster should be further split. If the second principal component is larger than one, the cluster is divided into two cluster components; otherwise, the procedure stops splitting.
2. Orthoblique rotation assigns each variable to the cluster components with which it has the higher squared correlation.
3. The variables are iteratively reassigned to clusters to maximize the variance accounted for by the cluster components.

4 Results and Discussion

4.1 *Time Courses of Near-Infrared Spectroscopy Signals*

An example of time courses of oxy-Hb signals measured from a single participant is shown in Fig. 3, and the channel

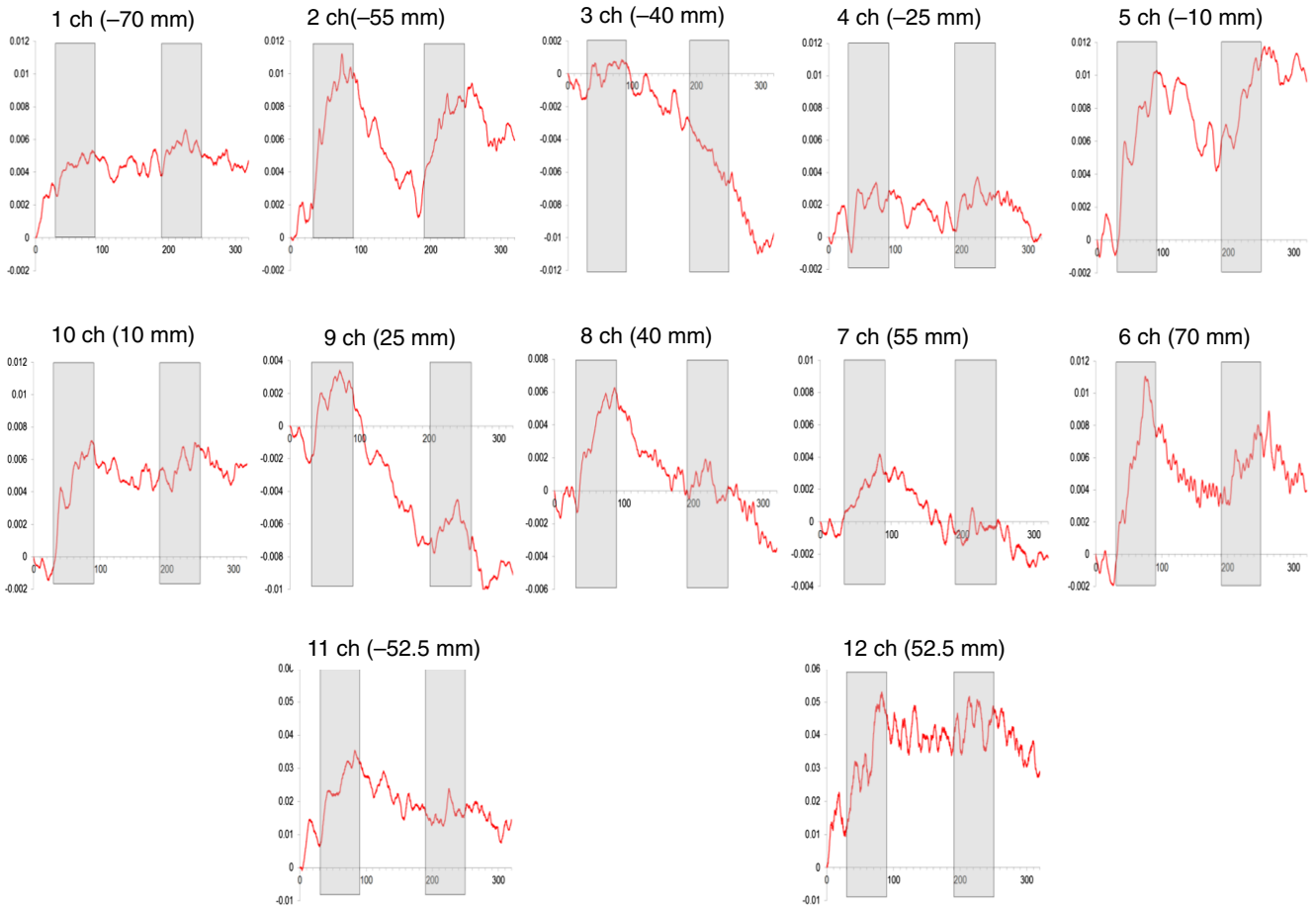

Fig. 3 Example time courses for the fNIRS (ch 1 to ch 10) signals and superficial (ch 11 and ch 12) oxy-Hb signals. The gray-shaded regions indicate VFT periods. The number in parentheses for each channel represents the distance from the midsagittal line.

arrangements are shown in Fig. 2. The top and the middle rows in Fig. 3 correspond to the oxy-Hb signals of superficial layers on the right and the left sides of the forehead, respectively. The bottom row corresponds to the oxy-Hb signals of the fNIRS performed on the forehead. First, it should be noted that the intensities of the oxy-Hb signals on most of the channels significantly increase during the VFT.

The ch 11 fNIRS signal from the right side strongly correlates with the ch 7 ($r = 0.79$) and ch 8 ($r = 0.84$) signals from the superficial layers. The ch 12 fNIRS signal from the left side strongly correlates with the ch 1 ($r = 0.80$), ch 5 ($r = 0.73$), ch 6 ($r = 0.79$), and ch 10 ($r = 0.86$) signals from the superficial layers. These results confirm the results of the previous studies indicating that the fNIRS signals are contaminated with superficial signals. The ch 2 signal from the superficial layers is strongly correlated with the ch 5 ($r = 0.76$), ch 6 ($r = 0.89$), and ch 10 ($r = 0.77$) signals from the superficial layers. The ch 3 signal from the superficial layers is strongly correlated with the ch 7 ($r = 0.80$), ch 8 ($r = 0.77$), and ch 9 ($r = 0.88$) signals from the superficial layers. Interestingly, however, the ch 2 signal has no correlation with the ch 3 ($r = -0.1$) signal. This result suggests that the spatial distribution of superficial signals from the forehead is heterogeneous. Accordingly, it is not possible to assume a spatial uniformity of superficial signals when one measurement area is far from another (i.e., at least by 15 mm).

4.2 *Task Performances*

First, the differences between the first- and second-task blocks in terms of group means of task performances [Fig. 4(a)], integral values of fNIRS oxy-Hb signal [Fig. 4(b)], and integral values of the superficial oxy-Hb signal [Fig. 4(c)] were compared. The integral value describes the size of the hemodynamic response during 60-s activation task periods.[38] The task performance for the second-task block improved slightly compared to that for the first-task block [average (SD): 16.7 (3.5) for the first task and 18.1 (3.2) for the second task]. The integral values of both the fNIRS and the superficial signals for the second-task block decreased compared to those for the first-task block. However, the first- and second-task blocks show no statistically significant difference in terms of either task performance or fNIRS signal strength ($P > 0.05$, paired t-test).

4.3 *Correlations Between Functional Near-Infrared Spectroscopy Signals and Superficial Signals*

To investigate the channel correlations between the fNIRS and superficial signals, color maps of the temporal cross-correlation coefficients between the oxy-Hb signals obtained from the fNIRS (FAR channels) and those from the superficial layer (NEAR channels) for each subject were produced (Fig. 5). The numbers (1 to 10) in the horizontal direction represent the channels of the superficial signals. The numbers (11 and 12) in the

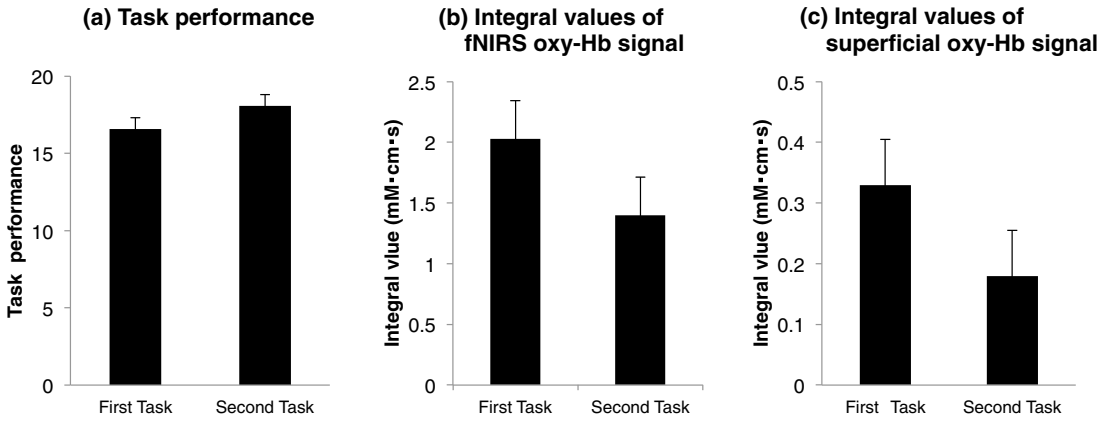

Fig. 4 Task performances and integral values of the fNIRS signals and superficial oxy-Hb signals. (a) Comparison of task performances between the first- and the second-task blocks, (b) comparison of the integral values of the fNIRS oxy-Hb signals between the first- and the second-task blocks, and (c) comparison of integral values of the superficial oxy-Hb signals between the first- and the second-task blocks. Error bars represent the standard error from the group average.

vertical direction represent the channels of the fNIRS signals. In the case of most subjects, the fNIRS signals (ch 11 and ch 12) are strongly correlated with the superficial signals even in a remote location of measurement channels, though the ch 11 and ch 12 signals are, respectively, located at positions including the ch 1, ch 2, and ch 3 signals and ch 6, ch 7, and ch 8 signals (which are the measured superficial layer signals, respectively). For example, in the case of subject 1, the fNIRS signal of ch 11 is strongly correlated with those of ch 6 and ch 7 as well as those of ch 1 and ch 2, though the ch 6 and ch 7 signals are located at positions on the opposite side (>100 mm from the position of the ch 11 signal). This result suggests possible existence of an anatomical structure through which fNIRS signals propagate to remote locations in the place.

4.4 *Spatial Distributions of Superficial Signals*

To investigate spatial distributions of the superficial signals, color maps of the temporal cross-correlation coefficients between the oxy-Hb signals from the superficial layer (NEAR channels) for each subject were produced (Fig. 6). The numbers (1 to 10) at the base of the color map represent the channels of the superficial signals. The cross-correlation matrix consists of 45 elements (the number of combinations of two channels selected from the 10 channels). The vertical direction (layer) of the color map represents the nearest order of the nearest-neighbor classification. Specifically, the bottom layer represents the temporal cross correlations between the NIRS signals on the nearest-neighbor channels, and the top layer represents the temporal cross correlation between the ch 1 and ch 6 signals. In addition, the horizontal direction of the color map represents the spatial distribution of the interchannel correlation of superficial signals from each layer, because the color map corresponds to the spatial position of a signal. Note that several subjects (except subjects 5, 6, 8, and 15) show low values (green or blue) of temporal cross-correlation coefficients of the signals from the bottom layer. These results mean that the assumption of homogeneous superficial signals does not stand in the case of any region of interest on the forehead with diameter of 15 mm or larger. In addition, the temporal cross-correlation coefficients for the lower layer (short-distance channels) are not necessarily higher than those for the upper layer (long-distance channels). These results indicate that the spatial distributions of hemoglobin signals from the superficial layers on the forehead are heterogeneous and mottled.

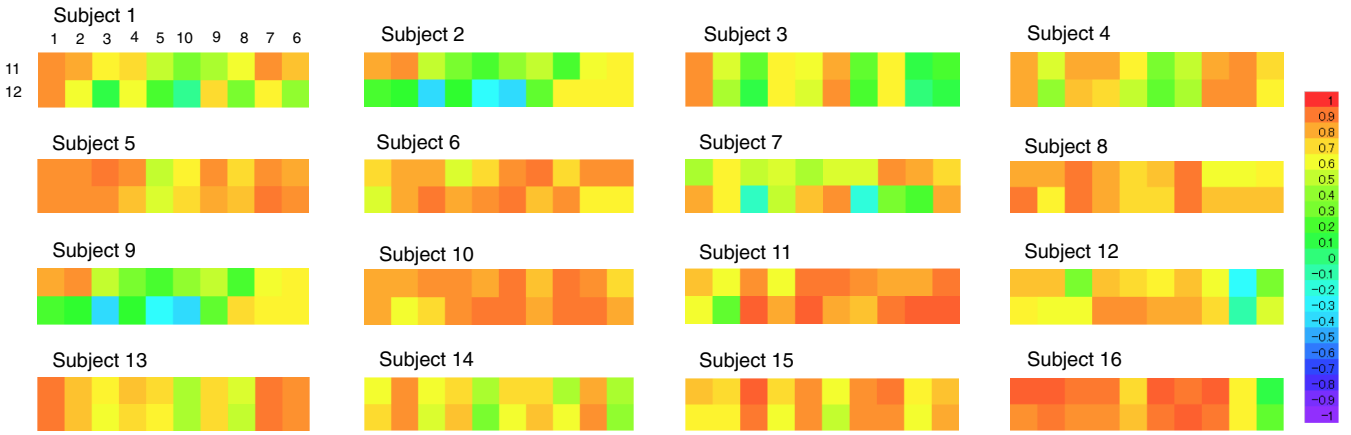

Fig. 5 Color maps of the temporal cross-correlation coefficients between the fNIRS oxy-Hb signals (FAR channels) and the superficial oxy-Hb signals (NEAR channels) for each of all individual subjects. Each row (1 to 10) and each column (11 and 12) in a color map represent FAR channel and NEAR channel, respectively.

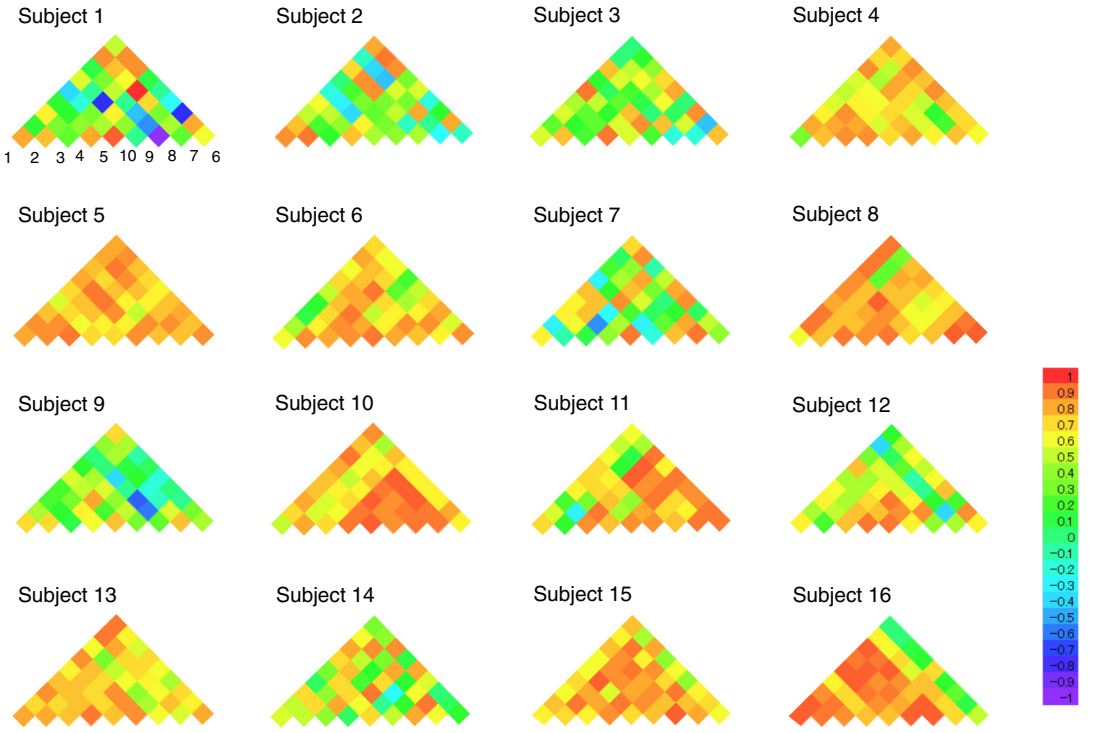

Fig. 6 Color maps of the temporal cross-correlation coefficients for the superficial oxy-Hb signals (NEAR channels) for each of all individual subjects. The numbers (1 to 10) at the base in the horizontal direction represent the NEAR channels.

CSU of the oxy-Hb signals from the superficial layer for each subject [calculated by mathematical Eq. (1)] are shown in Fig. 7. These results indicate that the spatial distributions of the superficial signals from the forehead vary significantly across subjects.

4.5 *Hierarchical Clustering of Temporal Cross Correlation Between Near-Infrared Spectroscopy Signals*

To investigate the structure of temporal cross correlation between the fNIRS and superficial signals on the channels, hierarchical clustering of the correlation was performed. Dendrograms of the hierarchical clustering for each subject are shown in Fig. 8. Although the dendrograms show a variety of patterns across the subjects, they can be classified into four types by the number of the clusters (cluster type 1: subjects 5 and 10; cluster type 2: subjects 4, 6, 7, 8, 11, 13, 14, 15, and 16; cluster type 3: subjects 1, 2, 3, and 12; and cluster type 4: subject 9).

To understand the physiological meaning of these dendrograms, network graphs of the NIRS signals of all subjects, which are new dendrograms without changing order of the spatial positions of the channels, were created. Typical network graphs of hierarchical clustering classified into the four types are shown in Fig. 9. The frontal branches of superficial temporal vessels run tortuously upward or downward and forward or backward to the

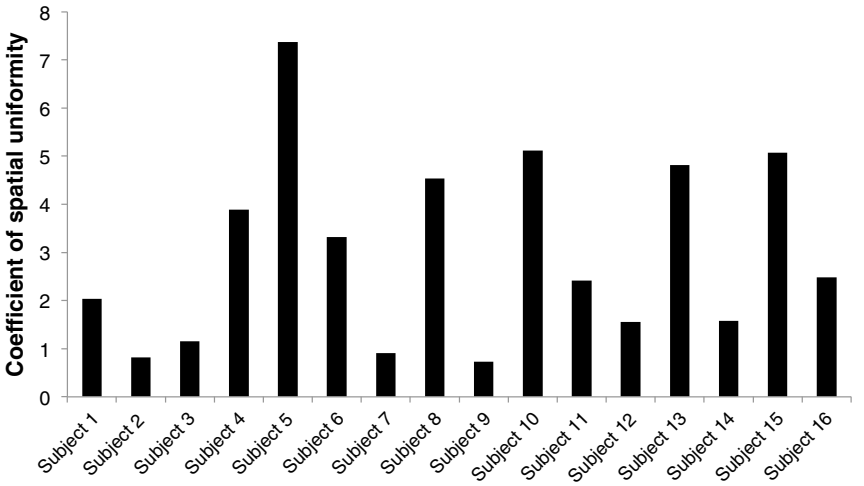

Fig. 7 Bar graphs of the coefficient of temporal–spatial uniformity calculated using Eq. (1) for each subject.

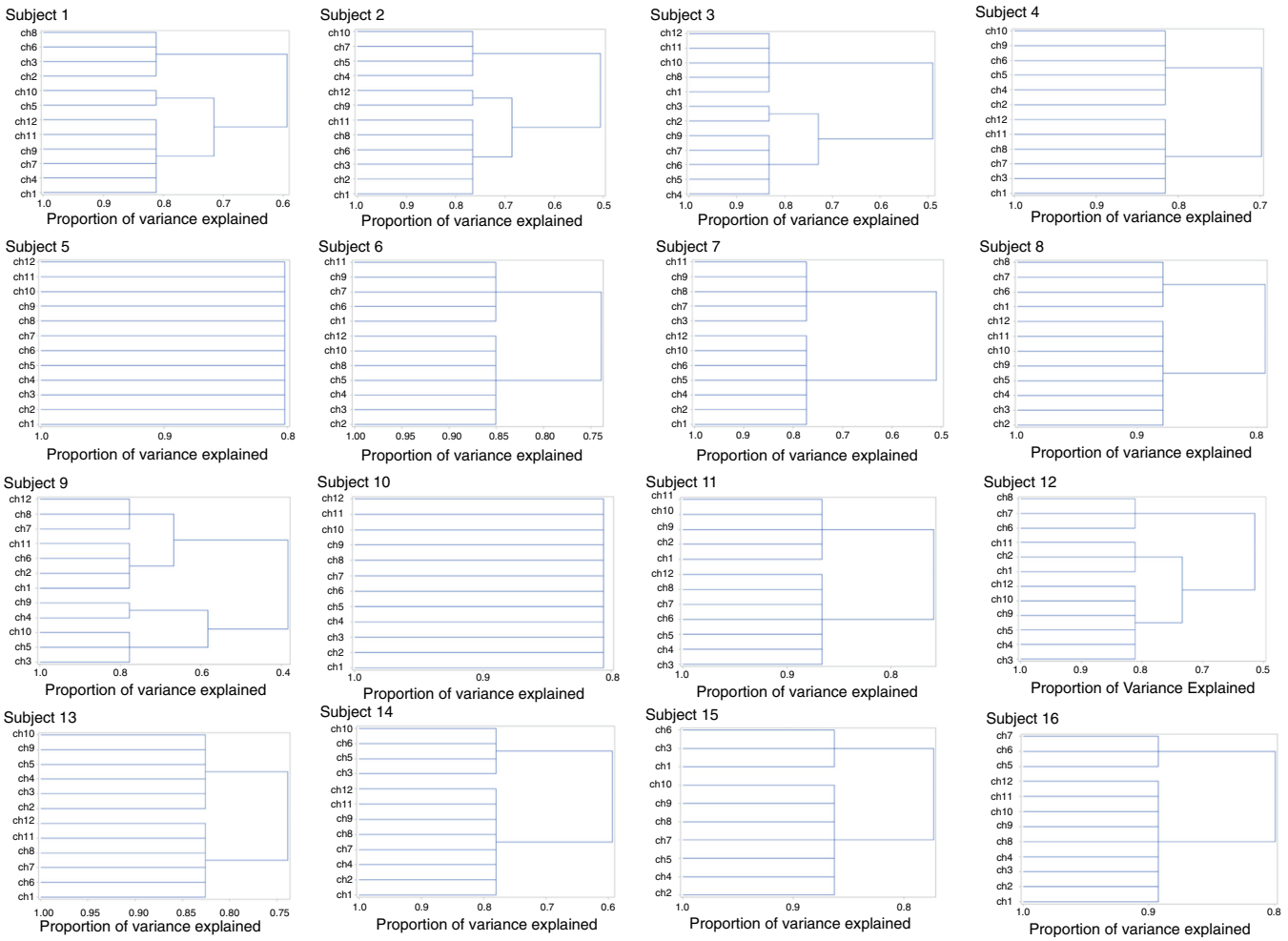

Fig. 8 Dendrograms of hierarchical clustering of temporal cross correlation between NIRS signals for each subject.

forehead, supplying the muscles, integument, and pericranium in this region, and anastomosing with the supraorbital and supratrochlear vessels. The superficial temporal artery is one of the temporal branches of the external carotid artery. On the other hand, the supraorbital and supratrochlear arteries derive from the ophthalmic artery, which is derived from the internal carotid artery. The supratrochlear artery exhibits a more superficial course and has a larger diameter than the supraorbital artery [1.08 ± 0.19 mm cf. 0.86 ± 0.19 mm (SD)].[44] The fNIRS signal is extremely vulnerable to contamination by changes in blood flow of these vessels in the dermis and hypodermis because the sensitivity in the superficial layers is higher than that in the deeper layer.[24] Time-resolved-reflectance measurements on a heterogeneous tissue-vessel model have revealed that the influence of blood vessels on the absorption coefficient is formulated as a function proportional to the vessel-to-brain volume ratio, which includes an exponential decay term of vessel diameter.[45] The fNIRS signals recorded on the forehead can, therefore, be contaminated by the superficial signals originating in these vessels to various degrees. Furthermore, anatomical variations occur in the supratrochlear and supraorbital arteries: the average distance between the exit of the supratrochlear artery and the midline was found to be 16.4 ± 1.7 mm (range, 13 to 20), and the average distance between the exit of the supraorbital artery and the midline measured 26.5 ± 2.6 mm (range, 23 to 35).[44] It has also been reported that the supraorbital artery may be absent in 10% to 20% of individuals.[46] Like the arteries, the external veins of the head and face show significant variations in morphology, size, and termination. The facial vein receives the supratrochlear and supraorbital veins and descends obliquely behind the facial artery.[47] Taking these reported results together with the results of this study suggest that the network structures of hierarchical clustering shown in Fig. 9 represent the vascular network structure accompanying anatomical variations. Since the VFT has been used in the aiding the differential diagnosis of depressive symptoms approved officially as the medical insurance coverage by the Ministry of Health, Labor, and Welfare of Japan in 2014, we have focused on the VFT in this study. It is conceivable that the superficial signals vary with kinds of tasks and/or task designs. Thus, it should be noted that the cluster patterns shown in Fig. 9 might be specific to the present experimental conditions.

5 Conclusions

It was observed that fNIRS signals recorded during a letter-cued VFT strongly correlate with the superficial signals even in a remote location of measurement channels. It was also observed spatial heterogeneous distributions and network structures of superficial signals appear across the forehead. These results suggest that the spatial heterogeneous distributions of the

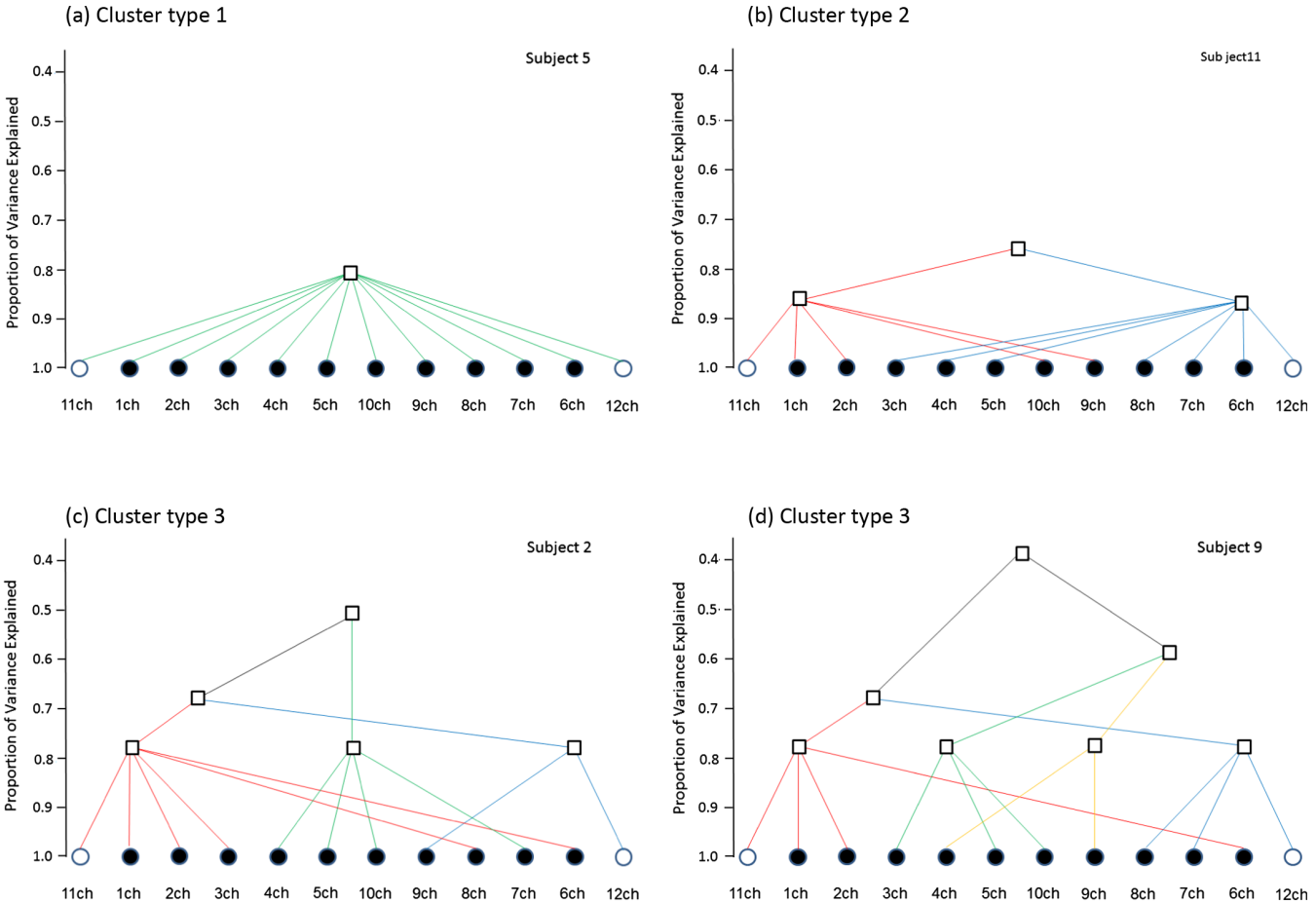

Fig. 9 Network structures of hierarchical clustering of temporal cross correlations between the channels (fNIRS and superficial signals). The network structures are classified into four types according to the numbers of the cluster hierarchy: (a) cluster type 1, (b) cluster type 2, (c) cluster type 3, and (d) cluster type 4.

superficial signals may be accounted for by vascular networks mainly consisting of supraorbital, supratrochear, and superficial temporal vessels.

Acknowledgments

The authors thank Professor Y. Ohashi for his help with the hierarchical cluster analysis using the VARCLUS procedure.

References

1. F. F. Jobsis, "Noninvasive, infrared monitoring of cerebral and myocardial oxygen sufficiency and circulatory parameters," *Science* **198**(4323), 1264–1267 (1977).
2. Y. Hoshi, "Towards the next generation of near-infrared spectroscopy," *Philos. Trans. R. Soc. London Ser. A* **369**(1955), 4425–4439 (2011).
3. M. Ferrari and V. Quaresima, "A brief review on the history of human functional near-infrared spectroscopy (fNIRS) development and fields of application," *NeuroImage* **63**(2), 921–935 (2012).
4. B. Chance et al., "Cognition-activated low-frequency modulation of light absorption in human brain," *Proc. Nat. Acad. Sci. U.S.A.* **90**(8), 3770–3774 (1993).
5. Y. Hoshi and M. Tamura, "Detection of dynamic changes in cerebral oxygenation coupled to neuronal function during mental work in man," *Neurosci. Lett.* **150**(1), 5–8 (1993).
6. T. Kato et al., "Human visual cortical function during photic stimulation monitoring by means of near-infrared spectroscopy," *J. Cerebral Blood Flow Metab.* **13**(3), 516–520 (1993).
7. A. Villringer et al., "Near infrared spectroscopy (NIRS): a new tool to study hemodynamic changes during activation of brain function in human adults," *Neurosci. Lett.* **154**(1–2), 101–104 (1993).
8. H. R. Heekeren et al., "Cerebral haemoglobin oxygenation during sustained visual stimulation—a near-infrared spectroscopy study," *Philos. Trans. R. Soc. London Ser. B* **352**(1354), 743–750 (1997).
9. Y. Hoshi et al., "Recognition of human emotions from cerebral blood flow changes in the frontal region: a study with event-related near-infrared spectroscopy," *J. Neuroimaging* **21**(2), e94–e101 (2011).
10. J. H. Meek et al., "Regional changes in cerebral haemodynamics as a result of a visual stimulus measured by near infrared spectroscopy," *Proc. Biol. Sci.* **261**(1362), 351–356 (1995).
11. K. Sakatani et al., "Cerebral blood oxygenation changes induced by auditory stimulation in newborn infants measured by near infrared spectroscopy," *Early Hum. Dev.* **55**(3), 229–236 (1999).
12. A. Seiyama et al., "Circulatory basis of fMRI signals: relationship between changes in the hemodynamic parameters and BOLD signal intensity," *NeuroImage* **21**(4), 1204–1214 (2004).
13. W. N. Colier et al., "Human motor-cortex oxygenation changes induced by cyclic coupled movements of hand and foot," *Exp. Brain Res.* **129**(3), 457–461 (1999).
14. C. Hirth et al., "Non-invasive functional mapping of the human motor cortex using near-infrared spectroscopy," *NeuroReport* **7**(12), 1977–1981 (1996).
15. A. Kleinschmidt et al., "Simultaneous recording of cerebral blood oxygenation changes during human brain activation by magnetic resonance imaging and near-infrared spectroscopy," *J. Cerebral Blood Flow Metab.* **16**(5), 817–826 (1996).
16. I. Miyai et al., "Cortical mapping of gait in humans: a near-infrared spectroscopic topography study," *NeuroImage* **14**(5), 1186–1192 (2001).

17. I. Miyai et al., "Premotor cortex is involved in restoration of gait in stroke," *Ann. Neurol.* **52**(2), 188–194 (2002).
18. M. Suzuki et al., "Prefrontal and premotor cortices are involved in adapting walking and running speed on the treadmill: an optical imaging study," *NeuroImage* **23**(3), 1020–1026 (2004).
19. A. J. Fallgatter and W. K. Strik, "Reduced frontal functional asymmetry in schizophrenia during a cued continuous performance test assessed with near-infrared spectroscopy," *Schizophr. Bull.* **26**(4), 913–919 (2000).
20. F. Okada et al., "Impaired interhemispheric integration in brain oxygenation and hemodynamics in schizophrenia," *Eur. Arch. Psychiatry Clin. Neurosci.* **244**(1), 17–25 (1994).
21. A. J. Fallgatter et al., "Loss of functional hemispheric asymmetry in Alzheimer's dementia assessed with near-infrared spectroscopy," *Brain Res. Cognit. Brain Res.* **6**(1), 67–72 (1997).
22. E. B. Hanlon et al., "Near-infrared fluorescence spectroscopy detects Alzheimer's disease in vitro," *Photochem. Photobiol.* **70**(2), 236–242 (1999).
23. C. Hock et al., "Near infrared spectroscopy in the diagnosis of Alzheimer's disease," *Ann. N.Y. Acad. Sci.* **777**, 22–29 (1996).
24. F. B. Haeussinger et al., "Simulation of near-infrared light absorption considering individual head and prefrontal cortex anatomy: implications for optical neuroimaging," *PloS One* **6**(10), e26377 (2011).
25. S. Kohno et al., "Removal of the skin blood flow artifact in functional near-infrared spectroscopic imaging data through independent component analysis," *J. Biomed. Opt.* **12**(6), 062111 (2007).
26. T. Takahashi et al., "Influence of skin blood flow on near-infrared spectroscopy signals measured on the forehead during a verbal fluency task," *NeuroImage* **57**(3), 991–1002 (2011).
27. S. Koike et al., "Near-infrared spectroscopy in schizophrenia: a possible biomarker for predicting clinical outcome and treatment response," *Front. Psychiatry* **4**, 145 (2013).
28. Y. Zhang et al., "Eigenvector-based spatial filtering for reduction of physiological interference in diffuse optical imaging," *J. Biomed. Opt.* **10**(1), 011014 (2005).
29. L. Gagnon et al., "Improved recovery of the hemodynamic response in diffuse optical imaging using short optode separations and state-space modeling," *NeuroImage* **56**(3), 1362–1371 (2011).
30. R. B. Saager and A. J. Berger, "Direct characterization and removal of interfering absorption trends in two-layer turbid media," *J. Opt. Soc. Am. A* **22**(9), 1874–1882 (2005).
31. T. Yamada, S. Umeyama, and K. Matsuda, "Multidistance probe arrangement to eliminate artifacts in functional near-infrared spectroscopy," *J. Biomed. Opt.* **14**(6), 064034 (2009).
32. Q. Zhang, E. N. Brown, and G. E. Strangman, "Adaptive filtering to reduce global interference in evoked brain activity detection: a human subject case study," *J. Biomed. Opt.* **12**(6), 064009 (2007).
33. Y. Zhang, J. Sun, and P. Rolfe, "Reduction of global interference in functional multidistance near-infrared spectroscopy using empirical mode decomposition and recursive least squares: a Monte Carlo study," *J. Eur. Opt. Soc.* **6**, 11033 (2011).
34. A. Jelzow et al., "Separation of superficial and cerebral hemodynamics using a single distance time-domain NIRS measurement," *Biomed. Opt. Express* **5**(5), 1465–1482 (2014).
35. C. Sato et al., "Intraoperative monitoring of depth-dependent hemoglobin concentration changes during carotid endarterectomy by time-resolved spectroscopy," *Appl. Opt.* **46**(14), 2785–2792 (2007).
36. E. Kirilina et al., "The physiological origin of task-evoked systemic artefacts in functional near infrared spectroscopy," *NeuroImage* **61**(1), 70–81 (2012).
37. L. Gagnon et al., "Short separation channel location impacts the performance of short channel regression in NIRS," *NeuroImage* **59**(3), 2518–2528 (2012).
38. R. Takizawa et al., "Neuroimaging-aided differential diagnosis of the depressive state," *NeuroImage* **85**(Pt. 1), 498–507 (2014).
39. D. T. Delpy et al., "Estimation of optical pathlength through tissue from direct time of flight measurement," *Phys. Med. Biol.* **33**(12), 1433–1442 (1988).
40. S. J. Matcher et al., "Performance comparison of several published tissue near-infrared spectroscopy algorithms," *Anal. Biochem.* **227**(1), 54–68 (1995).
41. G. M. Savitzky, "Smoothing and differentiation of data by simplified least squares procedures," *Anal. Chem.* **36**, 1627–1639 (1964).
42. D. A. Boas, A. M. Dale, and M. A. Franceschini, "Diffuse optical imaging of brain activation: approaches to optimizing image sensitivity, resolution, and accuracy," *NeuroImage* **23**(Suppl. 1), S275–S288 (2004).
43. SAS Institute Inc., "SAS/STAT® 13.2 User's Guide," 2014, SAS Institute Inc., Cary, North Carolina, https://support.sas.com/documentation/onlinedoc/stat/132/varclus.pdf.
44. O. K. Schwenn et al., "Experimental percutaneous cannulation of the supraorbital arteries: implication for future therapy," *Invest. Ophthalmol. Visual Sci.* **46**(5), 1557–1560 (2005).
45. H. Liu et al., "Influence of blood vessels on the measurement of hemoglobin oxygenation as determined by time-resolved reflectance spectroscopy," *Med. Phys.* **22**(8), 1209–1217 (1995).
46. J. J. Dutton, "Atlas of clinical and surgical orbital anatomy," in *Extra Orbital Branches of the Ophthalmic Artery*, p. 280, Saunders (2011).
47. E. T. Peuker, G. Fischer, and T. J. Filler, "Facial vein terminating in the superficial temporal vein: a case report," *J. Anat.* **198**(Pt. 4), 509–510 (2001).

Satoru Kohno received his BSc and MSc degrees in applied physics from Miyazaki University. He is an associate professor in the Department of Radiation Science and Technology, Tokushima University Graduate School. After working as a scientist and engineer at instrument companies, he received his PhD in medicine from the Graduate School of Medicine, Kyoto University. He developed magnetic resonance imaging and functional near-infrared spectroscopy (fNIRS) equipment and received some 40 patents.

Yoko Hoshi received her master's degree graduated from Akita University School of Medicine and got her medical license in 1981, and received her PhD from Hokkaido University in 1990. She is a pediatrician (a child neurologist), while she has also been participating in developing NIRS and research in cognitive neuroscience. Her recent research interest is developing diffuse optical tomography.